IOP Conf. Series: Materials Science and Engineering **389** (2018) 012027 doi:10.1088/1757-899X/389/1/012027

Three-Dimensional Analysis of the Effect of Out-Of-Plane Constraint on the Local Plastic Strain around Crack Front

Zhao Lingyan[1, *], Cui Yinghao[2] and Yang Fuqiang[1]

[1]School of Science, Xi'an University of Science and Technology, Xi'an 710054, China
[2]School of Mechanical Engineering, Xi'an University of Science and Technology, Xi'an 710054, China

*gloomy2@foxmail.com

Abstract. In the last few decades, constraint effects and plastic strain ahead of crack front have played important roles in stress corrosion cracking (SCC) behaviour of reactor pressure vessels (RPV) and pipes. At the same average J-integral, the local three-dimensional stress-strain fields around crack fronts were simulated, the effects of out-of-plane constraint (specimen thickness) on plastic strain, plastic zone and SCC driving force along crack fronts were analyzed. The results show that the strains of thinner specimens near the free surface are more sensitive to out-of-plane constraint effect. The strain gradients of thinner specimens are more sensitive to out-of-plane constraint, especially near the free surface. The results may be used in incorporating out-of-plane constraint effects in structures for improving structural integrity assessments and analyses of RPVs and pipes.

1. Introduction

Both fracture behaviour and constraint effects play important roles in structural integrity assessment and design, especially for integrity analyses of RPVs and pipes. As the resistance of structures against the crack-tip plastic deformation, constraints have attracted much attention in the research of material fracture behaviour. Constraints can be divided into in-plane constraint and out-of-plane constraint. The in-plane constraint, such as the crack length, relates to the specimen dimension in the direction of growing crack. While, the out-of-plane constraint, such as the specimen thickness, relates to the specimen dimension parallel to crack front. In the last few decades, many constraint parameters has been investigated to establish a unified correlation of in-plane and out-of-plane constraints with fracture toughness for improving structural integrity accuracy [1-3]. However, a great deal of evidence and experiments indicated that the material plasticity and residual plastic strain ahead of crack front also have great effect SCC behaviours of RPVs and pipes [4,5], which has been paid more attention in the nuclear power industry. In order to increase the accuracy of structural integrity assessment, the constraint effects on the plastic strain around crack fronts and the crack driving force must be considered.

At the same average J-integral, the local stress-strain fields ahead of crack fronts were calculated by using elastic-plastic finite element method (EPFEM). Moreover, the effect of out-of-plane constraint on plastic strain, plastic zone and SCC driving force along the specimen crack fronts were

Content from this work may be used under the terms of the Creative Commons Attribution 3.0 licence. Any further distribution of this work must maintain attribution to the author(s) and the title of the work, journal citation and DOI.
Published under licence by IOP Publishing Ltd

analyzed. The SCC crack growth rates of C(T) specimen with different thickness were also discussed in this paper.

2. Finite element modelling

2.1. Specimen model

A compact tension (CT) specimen with a constant load was used to measure SCC growth rate in high temperature water environment [6]. Five types of C(T) specimens (specimen width W=50 mm) with thickness-to-width ratio B/W=0.0625, 0.125, 0.25, 0.5 and 1 were chosen, and their relative crack length a/W=0.5 after pre-cracking. The geometry and size configurations of a C(T)50 specimen is shown in figure 1. It can be considered that the out-of-plane constraints were changed by the changing specimen thickness B, and the specimen sizes are shown in table 1.

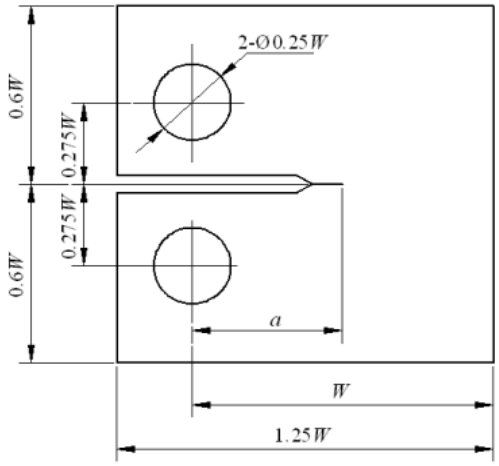

Figure1. Geometry of C(T)50 specimen (W=50 mm)

The calculated results of fracture toughness are also listed in table 1. The stress-strain field distributions along crack fronts were calculated at the same average J-integral value of J_{ave}=20 kJ/m^2 along the specimen crack fronts with different out-of-plane constraints, and the maximum values of J-internal J_{max} at the crack fronts mid-point were also listed. The values of fracture toughness K_{max} in table 1 were calculated from J_{max} by equation 1.

$$K_{\max} = \sqrt{J_{\max} \frac{E}{1-\nu^2}} \tag{1}$$

Where, E is the Young's modulus and ν is the Poisson's ratio.

Table 1. C(T) specimen sizes and the calculated results of fracture toughness

Specimen	a/W	B (mm)	B/W	P (kN)	K_{max} (MPa·m$^{1/2}$)	J_{max} (kJ·m^{-2})
C(T)50	0.5	3.125	0.0625	1.83	74.78	23.67
		6.25	0.125	3.7	74.56	23.53
		12.5	0.25	7.57	74.27	23.35
		25	0.5	15.6	74.05	23.21
		50	1	32.4	74.02	23.19

2.2. Material model

The pressure vessel steel 22NiMoCr3-7 is investigated in this paper, and its non-linear relationship between stress and strain beyond yield can be described by Ramberg-Osgood equation [7]:

$$\frac{\varepsilon}{\varepsilon_0} = \frac{\sigma}{\sigma_0} + \alpha \left(\frac{\sigma}{\sigma_0} \right)^n \tag{2}$$

Where ε is the strain, including elastic and plastic strain. σ is the total stress; ε_0 is the yield strain of the material, σ_0 is the yield stress of the material, and n is the strain hardening exponent of the material, α is the material offset coefficient.

The mechanical properties data and the Ramberg-Osgood constitutive parameters of 22NiMoCr3-7 steel at -60℃ are given in table 2.

Table 2. Mechanical properties of 22NiMoCr3-7 steel at -60℃[8]

Material	Young's modulus E (MPa)	Poison ratio ν	Yield stress σ_0 (MPa)	Hardening exponent n	Hardening parameter α
22NiMoCr3-7	215 000	0.3	517	3.7	6.2

2.3. FE Model

Five 3D finite element models in table 1 were built by the commercial finite element code ABAQUS [9]. The eight-node isoperimetric elements with reduced integration (C3D8R) were used for all models. To reduce the computation time, considering the loading and geometry symmetry, only 1/4th of the specimen was modeled. The symmetry boundary conditions were applied on the un-cracked ligaments. The finite element model meshes of C(T)50 specimen with B=25 mm and a/W=0.5 are shown in figure 2.

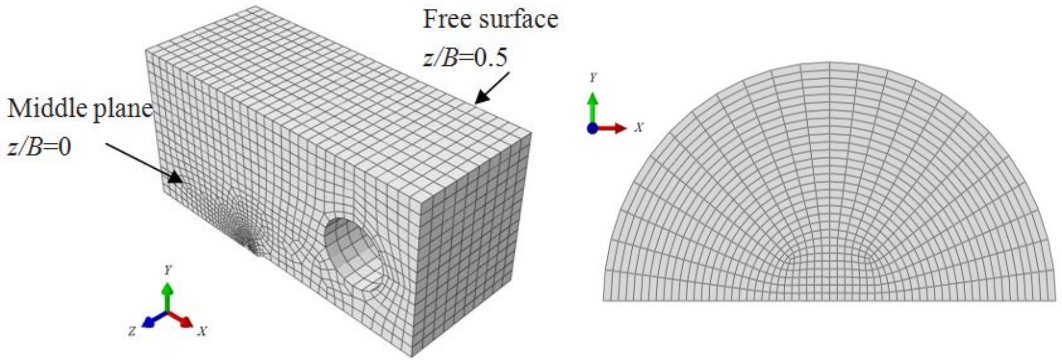

(a) Mesh of global model (b) Mesh around crack front

Figure 2. The global model mesh and mesh around crack front of C(T)50 specimen with B=25 mm and a/W=0.5

3. Results and Discussion

Mechanical affecting factors of crack driving force, such as plastic zone, plastic strain and plastic strain rate ahead of crack tips are crucial to quantitatively predict SCC growth rate. Therefore, to analyze the effect of out-of-plane constraint on the plastic strain along crack front, the 5 specimens with different out-of-plane constraints in table 1 were modelled and the local stress-strain fields around crack fronts with different specimen thickness were calculated by FEM. The loading condition is at the same average J-integral value of J_{ave}=20 kJ/m^2 along crack fronts (specimen thickness) for the C(T)50 specimens with different out-of-plane constraint in table 1.

3.1. Local strain zones around crack fronts

The equivalent plastic strain distributions around crack fronts are shown in figure 3, the radius of the researched zone is 0.5 mm. From figure 3(a) to (e), the high strain zones have similar distributions and the low strain zones decrease with the increasing specimen thickness B, which implies that the strains of the low strain zones are more sensitive to the out-of-plane constraints in the centre region.

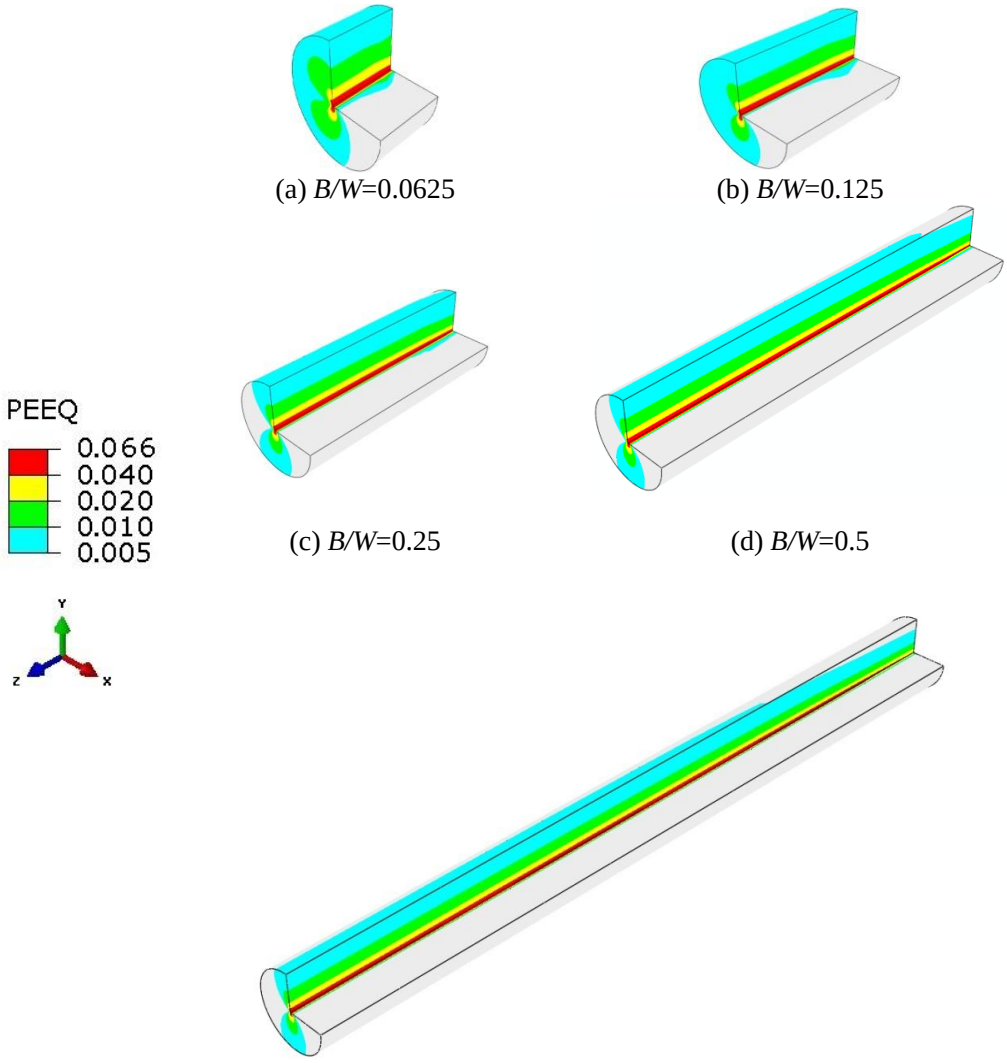

(a) *B/W*=0.0625 (b) *B/W*=0.125

(c) *B/W*=0.25 (d) *B/W*=0.5

(e) *B/W*=1

Figure3. Plastic strain zones around crack fronts at J_{ave}=20 kJ/m^2 with different *B/W*

3.2. Plastic strain curves along crack fronts

Figure 4 shows the equivalent plastic strain curves for C(T) specimens along crack fronts with the same *a*/*W*=0.5 (in-plane constraint) and different thickness B (out-of-plane constraint). The strains were calculated and evaluated at $r=2J/\sigma_0$ and $\theta=0$, where *r* is the distance from a crack tip and θ is the polar coordinate at the crack tip in the middle plane.

The curves are plotted against the normalized specimen thickness *z/B*, where *z/B*=0 means the middle plane and *z/B*=0.5 means the free surface of the specimens. It can be seen from figure 4 that the centre region (from *z/B*=0 to 0.4) of all specimens has lower strain, and the surface region (near *z/B* = 0.5) has higher strain. The stains along crack fronts of thicker specimens in the centre region (from *z/B*=0 to 0.3) have small variation while the stains of thinner specimens near the free surface (from *z/B*=0.3 to 0.5) have great variation with the increasing thickness B. This indicates that the strains of thinner specimens near the free surface are more sensitive to out-of-plane constraint effect induced by thickness B.

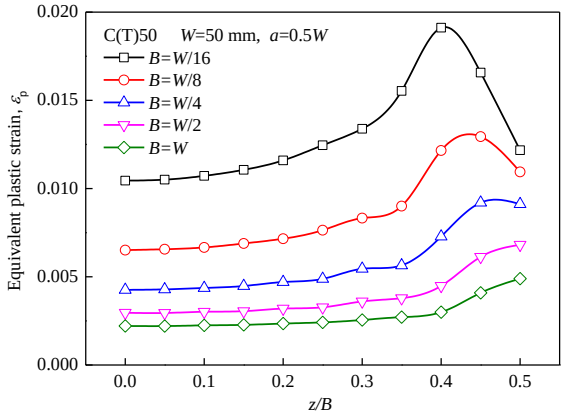

Figure 4. Equivalent plastic strain along crack fronts at J_{ave}=20 kJ/m^2

3.3. Plastic strain rate curves along crack fronts

In the film slip/dissolution oxidation model and FRI model of estimating SCC growth rate, the equivalent plastic strain rate can be used as the basic factor to quantitatively estimate SCC growth at flaws of actual LWR components in a specific high temperature oxygenated aqueous system [10]. Combined with the elastic-plastic FEM, the equivalent plastic strain gradient of a regular electrochemical environment where the crack fronts exposed can be calculated and the result curves are shown in figure 5.

The strain gradients along crack fronts in the centre region (from *z/B*=0 to 0.3) have small variation with the increasing thickness B, while the strain gradients of thinner specimens near the free surface (from *z/B*=0.3 to 0.5) are much higher than those of thicker specimens. It indicates that the SCC driving force decreases with the increasing thickness B, and the thinner specimens have much higher SCC crack growth rates than the thicker specimens at the same average J-integral. Figure 5 shows that the strain gradients of thinner specimens are more sensitive to out-of-plane constraint, especially near the free surface.

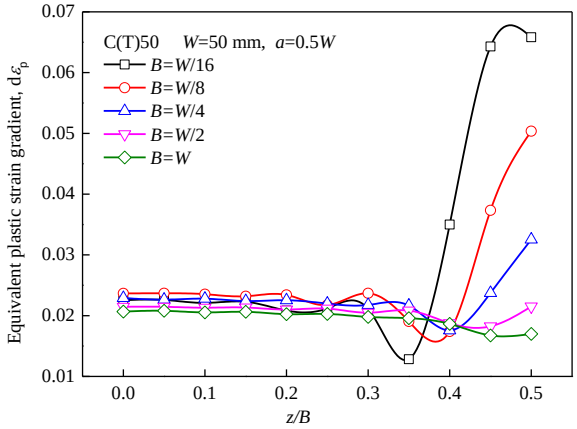

Figure 5. Equivalent plastic strain gradient along crack fronts at J_{ave}=20 kJ/m^2

4. Conclusion

Three-dimensional finite numerical simulations are carried out to analyze the stress-strain fields and plastic strain gradients along crack fronts with different out-of-plane constraints. The effect of out-of-plane constraint on crack driving force is also considered. Conclusions are as follows:

(1) The stains along crack fronts of thicker specimens in the centre region (from z/B=0 to 0.3) have small variation while the stains of thinner specimens near the free surface (from z/B=0.3 to 0.5) have great variation with the increasing thickness B. The strains of thinner specimens near the free surface are more sensitive to out-of-plane constraint effect induced by thickness B.

(2) SCC driving force decreases with the increasing thickness B, and the thinner specimens have much higher SCC crack growth rates than the thicker specimens at the same average J-integral. The strain gradients of thinner specimens are more sensitive to out-of-plane constraint, especially near the free surface.

Acknowledgements
This work is financially supported by the National Natural Science Foundation of China (Grant nos. are 11502195 and 51475362).

References

[1] Mu M Y, Wang G Z, Tu S T and XUAN F Z. (2016) Three-dimensional analyses of in-plane and out-of-plane crack-tip constraint characterization for fracture specimens. *Fatigue. Fract. Eng. M*., 39, pp1461-1476
[2] Yang J, Wang G Z, Xuan F Z and Tu S T. (2014) A unified correlation of in-plane and out-of-plane constraint with fracture resistance of a dissimilar metal welded joint. *Eng. Fract. Mech.*, 115, pp296-307
[3] Mu M Y, Wang G Z, Xuan F Z and Tu S T. (2015) Unified correlation of in-plane and out-of-plane constraints with cleavage fracture toughness. *Theor. Appl. Fract. Mec*., 80, pp121-132
[4] Li G F and Congleton J. (2000) Stress corrosion cracking of a low alloy steel to stainless steel transition weld in PWR primary waters at 292℃. *Corros. Sci.*, 42, pp1005-1021
[5] Li G F, Li G J, Fang K and Peng J. (2011) Stress corrosion cracking behavior of dissimilar metal weld A508/52M/316L in high temperature water environment. *Acta. Metall. Sin*., 47, pp797-803
[6] Kim Y J, Kim J S, Cho S M and Kim Y J. (2004) 3-D constraint effects on J, testing and crack tip constraint in M(T), SE(B), SE(T) and C(T) specimens: numerical study. *Eng. Fract. Mech*., 71, pp1203-1218
[7] Zhao L Y, Xue H, Yang F Q, Suo Y H. (2014) Numerical investigation on stress corrosion cracking behavior of dissimilar weld joints in pressurized water reactor plants. *Frat. Integrita Strutr*., 29, pp410-418
[8] Hebel, J., Hohe, J., Friedmann, V. and Siegele, D. (2007) Experimental and numerical analysis of in-plane and out-of-plane crack tip constraint characterization by secondary fracture parameters. *Int. J. Fract*., 146, pp173-188
[9] ABAQUS. (2015) ABAQUS/Standard User's Manual Version 6.14. *ABAQUS Inc*
[10] Xue H and Shoji T. (2007) Quantitative Prediction of EAC Crack Growth Rate of Sensitized Type 304 Stainless Steel in Boiling Water Reactor Environments Based on EPFEM. *J. Press. Vess.-T. ASME*, 129, pp460-467